Wu, Longfei, Longo, Alessandro, Dzade, Nelson Y. , Sharma, Akhil, Hendrix, Marco M. R. M., Bol, Ageeth A., De Leeuw, Nora H. , Hensen, Emiel J. M. and Hofmann, Jan Philipp 2019. The origin of high activity of amorphous MoS2 in the hydrogen evolution reaction. ChemSusChem 12 (19) , pp. 4383-4389. 10.1002/cssc.201901811

Publishers page: http://dx.doi.org/10.1002/cssc.201901811

# The Origin of High Activity of Amorphous $MoS_2$ in the Hydrogen Evolution Reaction

*Longfei Wu, Alessandro Longo, Nelson Y. Dzade, Akhil Sharma, Marco M. R. M. Hendrix, Ageeth A. Bol, Nora H. de Leeuw, Emiel J. M. Hensen*, and Jan P. Hofmann**

L. Wu, Prof. Dr. E. J. M. Hensen, Dr. J. P. Hofmann
Laboratory for Inorganic Materials and Catalysis, Department of Chemical Engineering and Chemistry, Eindhoven University of Technology, P.O. Box 513, 5600 MB Eindhoven, The Netherlands
E-mail: E.J.M.Hensen@tue.nl (Emiel J. M. Hensen) and J.P.Hofmann@tue.nl (Jan P. Hofmann)

Dr. A. Longo
Netherlands Organization for Scientific Research (NWO), The European Synchrotron Radiation Facility (ESRF), CS40220, 38043 Grenoble Cedex 9, France

Dr. N. Y. Dzade, Prof. Dr. N. H. De Leeuw
Faculty of Geosciences, Utrecht University, Princetonplein 9, 3584 CC Utrecht, The Netherlands; School of Chemistry, Cardiff University, Main Building, Park Place, CF10 3AT, Cardiff, United Kingdom

Dr. A. Sharma, Prof. Dr. A. A. Bol
Department of Applied Physics, Eindhoven University of Technology, P.O. Box 513, 5600 MB Eindhoven, The Netherlands

M. M. R. M. Hendrix
Laboratory of Physical Chemistry, Department of Chemical Engineering and Chemistry, Eindhoven University of Technology, P.O. Box 513, 5600 MB Eindhoven, The Netherlands

**Keywords**: proton reduction, $MoS_2$, polymorph, bond structure, *operando* XAS

## Abstract

Molybdenum disulfide ($MoS_2$) and related transition metal chalcogenides can replace expensive precious metal catalysts such as Pt for the hydrogen evolution reaction (HER). We investigated the relation between the nanoscale properties and HER activity of well-controlled 2H and Li-promoted 1T phases of $MoS_2$ as well as an amorphous $MoS_2$ phase. Our detailed comparison based on a Mo-S and Mo-Mo bond analysis under operando HER conditions reveals a similar bond structure in 1T and amorphous $MoS_2$ phases as a key feature in explaining their increased HER activity. Whereas the distinct bond structure in 1T phase $MoS_2$ is caused by $Li^+$ intercalation and disappears under harsh HER conditions, amorphous $MoS_2$ maintains its intrinsic short Mo-Mo bond feature and, with that, its high HER activity. Quantum-chemical calculations point at similar electronic structures of small $MoS_2$ clusters serving as models for amorphous $MoS_2$ and the 1T phase $MoS_2$ showing similar Gibbs free energies for hydrogen adsorption ($\Delta G_{H*}$) and metallic character.

Scalable electrochemical proton reduction (hydrogen evolution reaction, HER) is crucial for realizing large-scale storage of renewable energy. Water splitting requires efficient and robust catalysts, which are composed of earth abundant elements. The most active metal catalyst for HER is Pt, which is a scarce element making scale-up of water electrolysis to Terawatt (TW)-scale too costly.[1] Molybdenum disulfide ($MoS_2$), one of the most studied transition metal chalcogenides (TMCs), has received substantial attention because of its unique physiochemical properties such as a tunable band gap,[2] high catalytic activity,[3] and high electron mobility.[4] These properties allow it to be exploited in transistors,[5] metallo-enzymes,[6] and, at a practical scale, as the active phase in industrial catalysts for hydrotreating of oil fractions.[7] The ability to activate hydrogen reversibly also explains its promise for catalyzing the hydrogen evolution in the context of electrochemical water splitting.[8] Not surprisingly, the edge sites of $MoS_2$ nanocatalysts have been identified as active HER sites by Jaramillo and co-workers.[9] Since then, tremendous efforts have been devoted in engineering the surface structure of $MoS_2$ to preferentially expose these edge sites to improve HER performance.[10]

Different polymorphs of $MoS_2$ exist in the form of 2H (trigonally coordinated), 1T (octahedrally coordinated), and 3R phases (rhombohedral).[3, 11] 2H-$MoS_2$ is the thermodynamically stable two-dimensional (2D) phase with semiconductor properties (band gap ~1.9 eV for monolayer, 1.2 eV for bulk),[12] a low electron mobility and a limited number of HER active (edge) sites. These properties render this phase less attractive for electrocatalytic applications [2, 13] in comparison to the octahedral 1T phase, which is metallic and six orders of magnitude more conductive.[13a] The improved charge transfer kinetics as well as the affinity for binding H atoms on 1T-$MoS_2$ are reported to be responsible for the substantially enhanced HER activity compared to the 2H phase. However, the underlying mechanism of the high HER activity of the 1T phase has yet to be elucidated.[14] As the 1T phase can be formed from 2H-$MoS_2$ via intercalation of cations ($Li^+$, $Na^+$, etc.)[15], it is usually characterized by distorted structural domains.[16] Aside from 2H and 1T phases, amorphous $MoS_x$ (x = 2-3) has also been extensively investigated in the past as a hydrotreating catalyst and as a cathode material in lithium ion batteries.[17] Furthermore, it has recently been reported by Hu and other groups that this form of $MoS_2$ is a highly active electrocatalyst for HER.[8b, 18] While Mo edge sites of 2H-$MoS_2$ have been experimentally identified as the active HER sites, the question what causes the superior catalytic performance of 1T and amorphous phase $MoS_2$ remains unclear, which adds to the challenge of unraveling the HER mechanism in amorphous $MoS_2$.[11, 17b, 17c, 19]

Here, we show how the structure and surface properties of 2H, 1T and amorphous $MoS_2$ influence the HER activity and stability by a combined theory as well as *ex situ* and *operando* X-ray spectroscopy approach. In comparison to 2H-$MoS_2$, shorter Mo-S and Mo-Mo bonds were observed in both 1T and amorphous $MoS_2$ thin film electrodes. Besides, both core level Mo 3d and valence band photoemission spectra indicate that 1T and amorphous phase $MoS_2$ exhibit a similar electronic structure. The short Mo-Mo bond in 1T phase $MoS_2$ is caused by lithium intercalation and gradually changes back to the 2H phase accompanied by a decrease in HER activity at high overpotentials. By contrast, amorphous $MoS_2$ (Am-$MoS_2$) retains its intrinsic (short)Mo-S and Mo-Mo bond structure as well as high HER activity after 24 h electrochemical testing under the same conditions. Electrochemical *operando* X-ray absorption spectroscopy was performed to probe the local bond and electronic structure of $MoS_2$ under HER conditions. The results show that the observed feature of short Mo-Mo bonds plays a key role in determining the activity of both 1T and amorphous phase $MoS_2$ electrocatalysts for HER.

2H- and amorphous $MoS_2$ films were prepared by plasma enhanced atomic layer deposition (PEALD) on glassy carbon plates at 450 and 250 °C respectively, while the 1T phase was synthesized via lithium intercalation of the as-deposited 2H-$MoS_2$ (see supporting information for details). The HER electrocatalytic activity of as-prepared $MoS_2$ films was assessed in 0.1 M $H_2SO_4$ in a typical three-electrode electrochemical cell. As shown in Figure 1, both cyclic voltammetry (CV) and linear sweep voltammetry (LSV) curves present higher current densities for 1T and amorphous $MoS_2$ as compared to the 2H phase. However, even though 1T and amorphous $MoS_2$ have comparable current densities initially, the catalytic activity of the 1T phase gradually decreases during the stability test, while Am-$MoS_2$ maintained its higher initial activity (Figure 1d). This particular behavior led us to investigate further the electronic and structural properties of the materials.

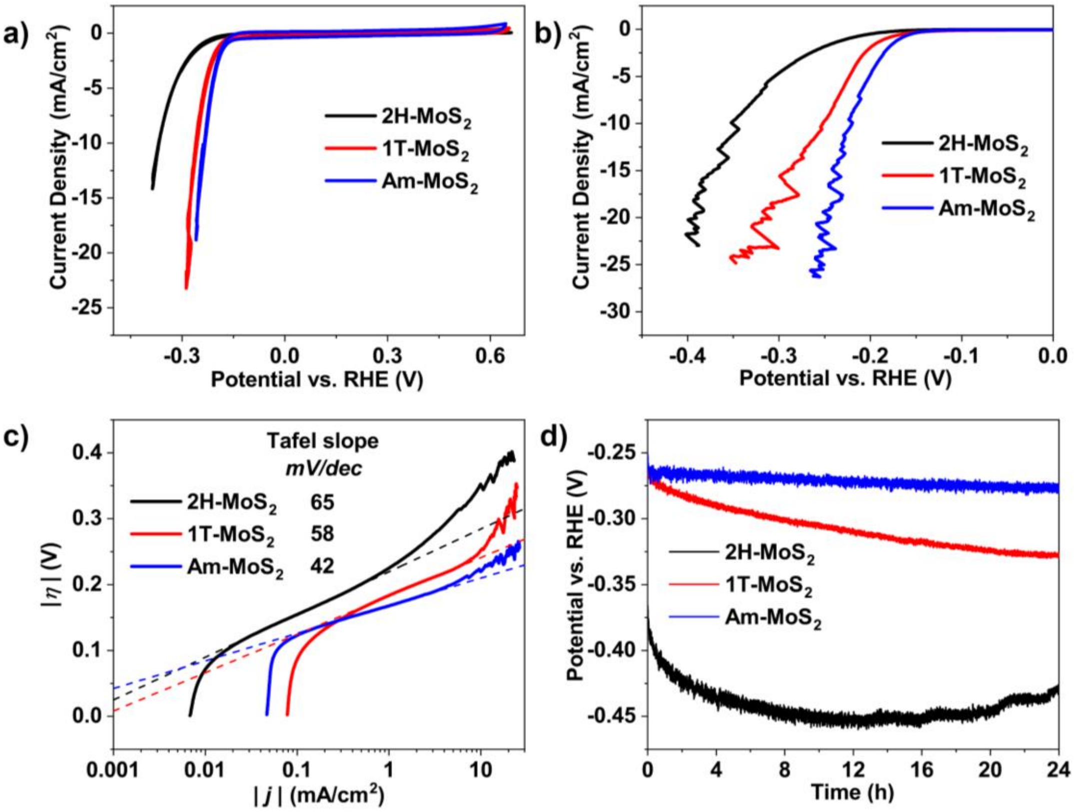

**Figure 1.** Cyclic voltammetry (CV, a) and linear sweep voltammetry (LSV, b) curves of 2H-, 1T- and Am-$MoS_2$ films corrected by uncompensated resistance with scan rates of 50 mV/s for CV and 5 mV/s for LSV; c) Tafel slopes obtained from LSV curves in (b); d) chronopotentiometric responses (*V*-*t*) recorded at a constant current density of 3 mA/cm$^2$. Electrolyte: 0.1 M $H_2SO_4$.

We used X-ray absorption spectroscopy at the Mo K-edge to probe the electronic as well as local geometric structure of these films. *Ex situ* X-ray absorption near edge spectra (XANES) of $MoS_2$ films before and after HER stability tests recorded under a grazing incidence angle of 0.3° (grazing incidence X-ray absorption spectroscopy)[23] are shown in

Figure 2. The suppression of features A and D in 1T (Figure 2d) compared to 2H-$MoS_2$ emphasizes its distinct bond structure. Importantly, feature A and D reappear for 1T-$MoS_2$ after 24 h HER stability test, which implies that the 1T phase is not stable under HER conditions and gradually changes back to 2H-$MoS_2$. In contrast, feature D is absent for amorphous (Figure 2g) phase compared to 2H-$MoS_2$ before and after HER, indicating its stable bond structure. Absorption edge features in the XANES spectra are very sensitive to the electronic properties of the atoms being probed:[20] the less expressed shoulder at the edge and the shift of the white line for 1T-$MoS_2$ compared to 2H-$MoS_2$ are indicative of the structural differences. Simulations of the Mo-K edge XANES spectra of $MoS_2$ with hexagonal (2H phase) and monoclinic (1T phase with Li intercalation) symmetry were performed to understand these differences. The red curves (Figure 2j, k) represent calculated spectra based on the model structure and the blue curves are calculated taking into account broadening by core-hole lifetime effects.[21] The fitted XANES spectra in both cases reproduce the experimental features of 2H- and 1T- $MoS_2$ well, which confirms their assignment. As monoclinic $MoS_2$ shows octahedral Mo coordination with a shorter bond distance than 2H-$MoS_2$ upon Li intercalation, we may conclude that the as-prepared 1T-$MoS_2$ in this study has a distorted bond structure. For further comparison, *ex situ* grazing incidence extended X-ray fine structure data (GI-EXAFS) of $MoS_2$ films were recorded before and after stability measurements. The Fourier transform (FT) profiles in R-space shown in Figure 2b and c present two main peaks at 2.40 Å and 3.16 Å (Table 1) corresponding to the nearest Mo-S and Mo-Mo bonds respectively. The CN values shown in Table 1 suggest that there is no complete shell of S atoms around the central Mo at the surface of the $MoS_2$ films, which can be due to termination by Mo edges or oxidation by emersion of the electrolyte and air exposure.[22] By contrast, FT curves of 1T-$MoS_2$ exhibit a distinct decrease of Mo-Mo bond length (short Mo-Mo bond) from 3.16 Å to 2.75 Å (Table 1), which corresponds to the characteristic bond length found in 1T phase $MoS_2$.[24, 25] Evidence for this feature can be also

found by the larger Debye-Waller ($\sigma^2$) factor of both Mo-S and Mo-Mo bonds in 1T phase compared to 2H-$MoS_2$ (Table S1) although the normal Mo-Mo bond (3.16 Å) is still present in 1T.[24] Nevertheless, this shortened Mo-Mo bond disappeared after 24 h HER stability testing, which is consistent with the observations from XANES that 1T changes back to 2H phase under these conditions. In the case of Am-$MoS_2$, a similarly short Mo-S and Mo-Mo bond structure was found (Figure 2h, i). The similarities between the 1T and amorphous phases in XANES and EXAFS are also reflected in the Mo 3d core level and valence band photoemission spectra (Figure S3, Tables S2 and S3), shifting consistently to lower binding energies. Therefore, we may suggest that the short Mo-Mo bond features observed in both 1T-$MoS_2$ and Am-$MoS_2$ play a key role in enhancing the HER activity of $MoS_2$ catalysts. Distinct from 1T phase, the short Mo-Mo bond in Am-$MoS_2$ was retained after 24 h of HER stability testing. Considering the HER stability of Am-$MoS_2$, we may conclude that the bond structure in Am-$MoS_2$ is intrinsic, *viz.* not caused by Li intercalation, resulting in a higher stability during 24 h HER stability testing.

Several structural models for amorphous $MoS_2$ or $MoS_3$ have been proposed in the literature by e.g. Hibble et al.[17b] and Weber et al.[11] [25] However, based on our experimental observations, we cannot conclusively assign a structure to Am-$MoS_2$. Nonetheless, the disorder in amorphous $MoS_2$ reported in this work is consistent with earlier reports.[17a, d] It is worth noting that even though the HER activity of 1T-$MoS_2$ decreases gradually (Figure 1d), the corresponding overpotential is still much lower than that of 2H-$MoS_2$, which we have recently attributed to the presence of remaining Li adsorbed on the 1T-$MoS_2$ even after loss of intercalated Li.[18c] ICP-OES analysis of $MoS_2$ films after stability tests confirms the presence of adsorbed Li on 1T-$MoS_2$ (Table S4), and the adsorption of Li on $MoS_2$ was observed to promote the activity of $MoS_2$ catalyzed hydrogen evolution reaction in our recent work. [18c]

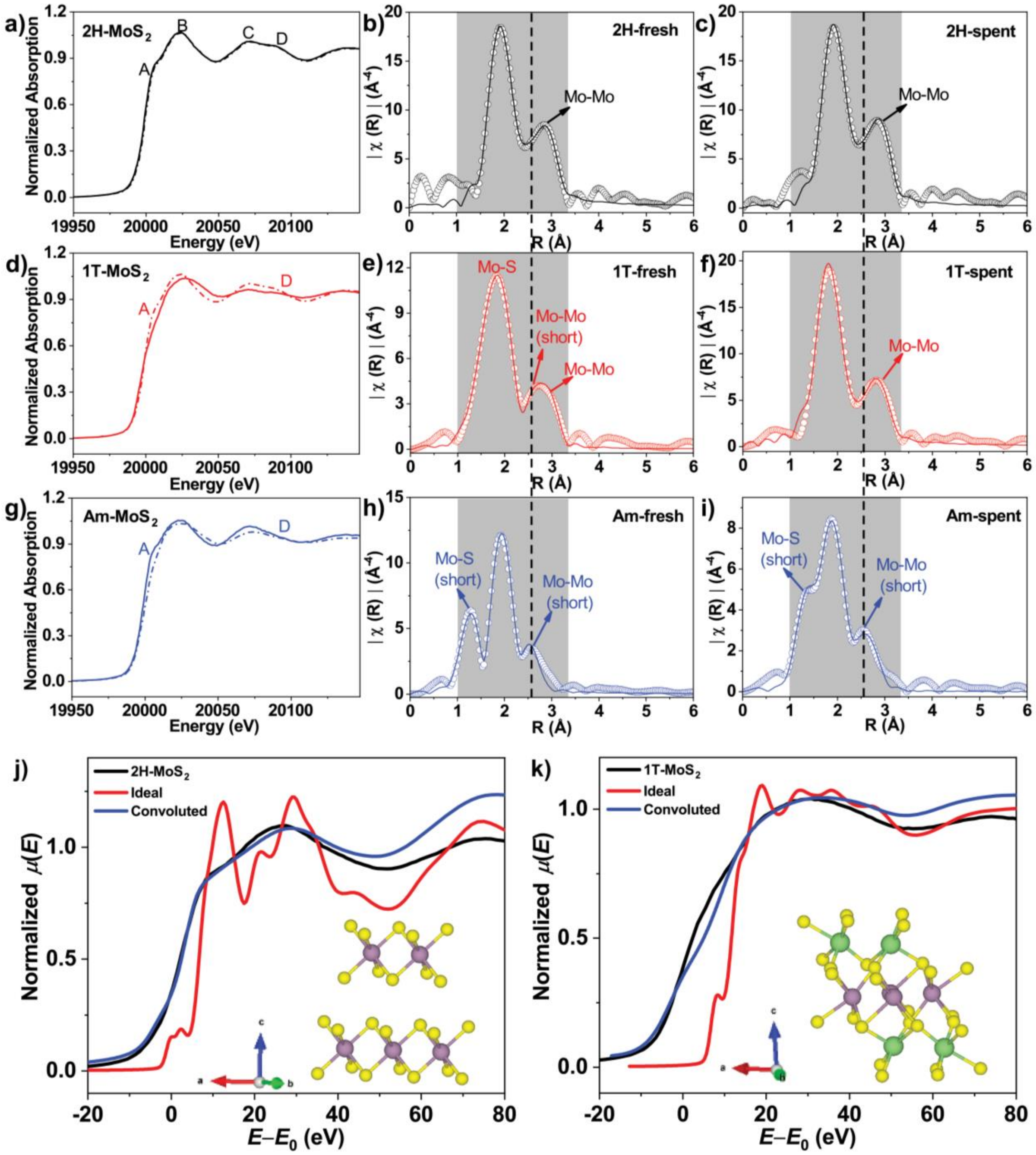

**Figure 2.** a, d, g) Mo K-edge XANES spectra of 2H-MoS$_2$ (a), 1T-MoS$_2$ (d), and Am-MoS$_2$ (g) before (solid line) and after (dash line) stability test; b, e, h) Mo K-edge Fourier transform EXAFS ($k^3$-weighted) of 2H-MoS$_2$ (b), 1T-MoS$_2$ (e), and Am-MoS$_2$ (h) before stability test; c, f, i) Mo K-edge Fourier transform EXAFS ($k^3$-weighted) of 2H-MoS$_2$ (c), 1T-MoS$_2$ (f), and Am-MoS$_2$ (i) after stability test; j, k) Mo-K edge XANES spectra of experimental data (black curve) and calculated simulation based on hexagonal (j, inset) and monoclinic (k, inset) structure model (purple, yellow and green balls corresponds to Mo, S and Li atoms, respectively), red curves represent simulated spectra while blue curves represent simulated spectra convoluted with the consideration of Mo 1s core-hole lifetime.

**Table 1.** Summary of the EXAFS spectroscopic features obtained for $MoS_2$ films under grazing incidence reflecting information about the top ~3 nm of the material.

| Sample | Shell | *ex-situ* grazing incidence Mo K-edge EXAFS[a)] | | | |
|---|---|---|---|---|---|
| | | Fresh | | Spent | |
| | | CN | R (Å) | CN | R (Å) |
| 2H-$MoS_2$ | Mo-S | 4.25 | 2.402 | 4.80 | 2.405 |
| | Mo-Mo | 2.26 | 3.155 | 2.98 | 3.158 |
| 1T-$MoS_2$ | Mo-S | 3.06 | 2.419 | 5.86 | 2.365 |
| | Mo-S (short) | 1.78 | 2.019 | - | - |
| | Mo-Mo | 1.70 | 3.148 | 2.26 | 3.145 |
| | Mo-Mo (short) | 0.96 | 2.748 | - | - |
| Am-$MoS_2$ | Mo-S | 5.29 | 2.430 | 3.50 | 2.368 |
| | Mo-S (short) | 0.60 | 1.767 | 0.56 | 1.802 |
| | Mo-Mo (short) | 1.08 | 2.778 | 1..57 | 2.824 |

[a)] Detailed fitting parameters can be found in Table S1.

To follow the structural evolution of the different $MoS_2$ catalysts under HER conditions, an *operando* electrochemical cell (Figure S5) was developed and applied for X-ray absorption spectroscopy experiments. The *operando* EXAFS spectra of different $MoS_2$ polymorphs in dry state and at set potentials of +0.3 V and −0.3 V vs. RHE in 0.1 M $H_2SO_4$ are shown in Figure 3. Table 2 summarizes the EXAFS fitting results. It can be seen that, despite a small reduction in coordination number (CN) for the Mo-Mo shell, the Mo-Mo and Mo-S bond distances as well as the Mo-S CN remained the same within the accuracy range, pointing at the overall structural stability of 2H-$MoS_2$ under HER conditions. For both 1T and Am-$MoS_2$, a shortened Mo-S bond could be identified as well. In contrast to the disappearance of short Mo-S and Mo-Mo bonds after the 24 h stability test (Figure 2), the *operando* EXAFS data of 1T-$MoS_2$ confirms the retention of short Mo-S bonds under various potentials. On the one hand, the *operando* XAS was not carried out at grazing incidence angle and therefore reflects mostly bulk film information. On the other hand, the *operando* XAS measurements were performed at −0.3 V *vs.* RHE with a current density of only −200 μA/cm$^2$ (Figure S6), while the 24 hours stability tests were performed at −3 mA/cm$^2$.

The surface electronic structure of 2H, 1T and amorphous $MoS_2$ films was probed by XPS before and after *operando* XAS measurements (Figure 3d, e). The Mo 3d core level component describing the Mo-S bond for pristine 1T and Am-$MoS_2$ was shifted negatively by ~0.9 eV compared to that of the 2H phase, which is a characteristic feature for both 1T and amorphous phase $MoS_2$.[18, 26] However, the core level of Mo(IV)-S (Mo $3d_{5/2}$ 228.6 eV) for 1T-$MoS_2$ shifted back to 229.5 eV after *operando* XAS tests, suggesting a transformation from 1T to 2H-$MoS_2$ at the surface. By contrast, the shift in Mo 3d core level spectra for Am-$MoS_2$ (~0.7 eV) remained unchanged after electrochemical tests (Figure 3d). Raman spectroscopy was then used to further support the presence of different $MoS_2$ phases.[16] As shown in Figure S18, there is a redshift of $E^1_{2g}$ and $A_{1g}$ peaks for 1T-$MoS_2$ compared to 2H-$MoS_2$, which stays constant before and after *operando* XAS measurements. The phase stability of the bulk 1T-$MoS_2$ film under mild reaction conditions is consistent with the EXAFS fitting results (Table 2). Even though sulfur dimers of Am-$MoS_2$ have been reported to be involved in proton reduction,[19c] the decreased intensity of sulfur dimers (Figure 3e) here apparently did not influence the HER activity (Figure S6).

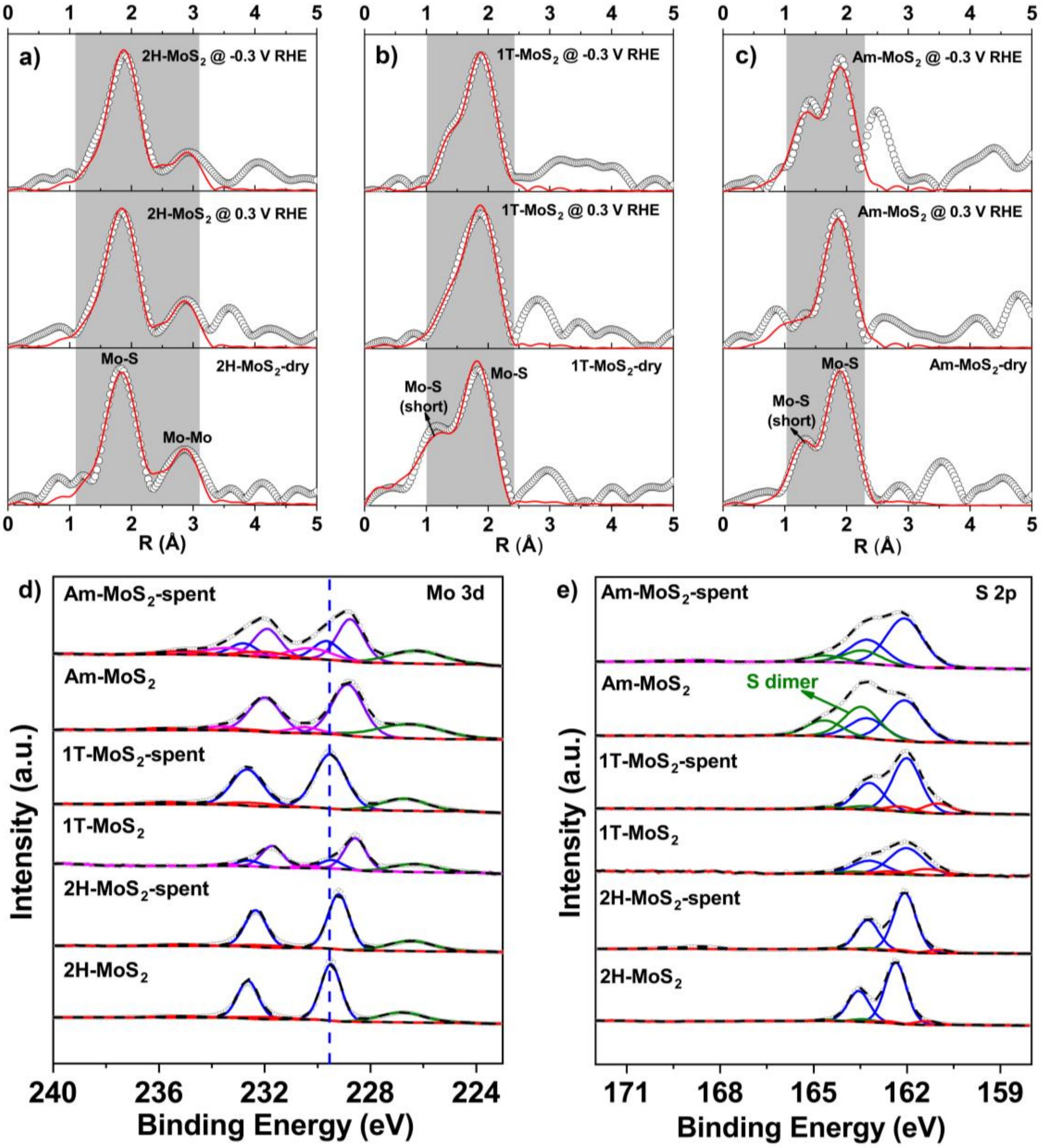

**Figure 3.** a-c) Mo K-edge Fourier transform EXAFS ($k^2$-weighted) of 2H- (a), 1T- (b) and Am- (c) $MoS_2$ under *operando* electrochemical conditions, grey region represents R-range for fitting; d, e) X-ray photoemission spectra of Mo 3d (d) and S 2p (e) before and after (-spent) *operando* XAS measurements.

**Table 2.** Summary of EXAFS spectroscopic features obtained for $MoS_2$ films under *operando* HER conditions.

| Sample | Shell | *ex-situ* grazing incidence Mo K-edge EXAFS[a)] | | | | | |
|---|---|---|---|---|---|---|---|
| | | Dry | | +0.3 V | | −0.3 V | |
| | | CN | R (Å) | CN | R (Å) | CN | R (Å) |
| $2H-MoS_2$ | Mo-S | 4.28 | 2.385 | 4.33 | 2.391 | 4.71 | 2.403 |
| | Mo-Mo | 3.06 | 3.154 | 2.70 | 3.142 | 2.11 | 3.165 |
| $1T-MoS_2$ | Mo-S | 6.66 | 2.354 | 5.82 | 2.416 | 3.78 | 2.406 |
| | Mo-S (short) | 5.90 | 2.004 | 0.96 | 1.835 | 0.34 | 1.827 |
| $Am-MoS_2$ | Mo-S | 4.60 | 2.443 | 3.04 | 2.401 | 2.30 | 2.407 |
| | Mo-S (short) | 0.36 | 1.775 | 0.38 | 1.644 | 0.58 | 1.795 |

[a)] Detailed fitting parameters can be found in Table S5, S6 and S7.

We utilized grazing incidence X-ray diffraction (GIXRD) to inspect the materials before and after *operando* XAS measurements. Figure S15 presents the diffraction patterns of $MoS_2$ films where the absence of diffraction peaks at 14.2° (002) and 33.3° (101) (2θ) for pristine 1T phase can be seen. However, the re-appearance of (002) and (101) reflections for the spent $1T-MoS_2$ sample suggests that the material gradually changes back to $2H-MoS_2$. In addition, SEM (scanning electron microscopy) images (Figure S16) reveal obvious morphology changes for the 1T phase after HER tests. By contrast, neither Raman (Figure S18) nor GIXRD show any peaks before and after HER test for $Am-MoS_2$. So far, we may conclude that even under mild HER conditions, the surface bond structure for 1T phase would disappear and change back to 2H phase, while amorphous $MoS_2$ retains its intrinsic short Mo-Mo bond feature and with that its high HER activity.

Using density functional theory (DFT), we compared the (electronic) structures of $Mo_3S_9$ and $Mo_6S_{17}$ clusters as a motif for $Am-MoS_2$ with those of $2H-MoS_2$ and $1T-MoS_2$ in order to understand differences in the Gibbs free energy of hydrogen adsorption ($\Delta G_{H*}$), which is considered as a relevant descriptor for HER activity.[13b, 27] The Mo−Mo and Mo−S bond distances found for the two small clusters correspond to those observed in $1T-MoS_2$ and are shorter than those in 2H-$MoS_2$ (Figure 4 and Figures S21 and S22). Together with the structural data derived from EXAFS for our samples, this provides good grounds to hypothesize that Am-$MoS_2$ consists of small $MoS_x$ clusters with an increased S/Mo ratio and shortened Mo-Mo and Mo-S bonds, similar to what is known for crystalline 1T-$MoS_2$. We then explored how these structures affect the HER performance for which we computed the Gibbs free energies of hydrogen adsorption ($\Delta G_{H^*}$, structures see Figures S23-S27). For optimum HER activity, the value of $\Delta G_{H^*}$ should be close to zero.[28] For $Mo_3S_9$, a $\Delta G_{H^*}$ of −0.06 eV was computed, which is much more favorable than values of +2.13 eV and +0.78 eV for the basal planes of 2H-$MoS_2$ and Li-stabilized 1T-$MoS_2$, respectively. As the hydrogen activation and formation on $MoS_2$ is known to occur at the edge terminations,[9a, 29] we also computed $\Delta G_{H^*}$ for hydrogen adsorption on the Mo-edges of 2H-$MoS_2$ (−0.23 eV) and 1T-$MoS_2$ (−0.10 eV). These data confirm that the edges of the distorted 1T-$MoS_2$ phase are the preferred sites for HER in comparison to the edges of 2H-$MoS_2$ and further suggest that small clusters also have a favorable $\Delta G_{H^*}$. Figure 4 also contains the partial density of states (PDOS, Figure 4d-g) of the two investigated clusters, 1T-$MoS_2$ and 2H-$MoS_2$. It can be immediately seen that, similar to 1T-$MoS_2$, the $Mo_3S_6$ and $Mo_6S_{17}$ cluster models exhibit metallic character with their Fermi level crossing the Mo 3d orbitals. In contrast, 2H-$MoS_2$ is a semiconductor with a band gap of 1.59 eV, which is consistent with valence band spectroscopy (Figures S12 and S13) and earlier theoretical predictions.[30, 31] The adsorption of hydrogen does not induce significant changes to the electronic structures, although coupling between H-*s* orbital and Mo-*d* and S-*p* orbitals is observed, consistent with weak bonding and high HER activity. The metallic nature of the $Mo_3S_6$, $Mo_6S_{17}$ clusters and 1T-$MoS_2$ results in a higher intrinsic electronic conductivity of these materials as compared to the semiconducting 2H-$MoS_2$. Therefore, in addition to a more optimum free energy for hydrogen adsorption, the enhanced HER activity of 1T-$MoS_2$ and Am-$MoS_2$ can be further rationalized by a higher intrinsic electronic conductivity.

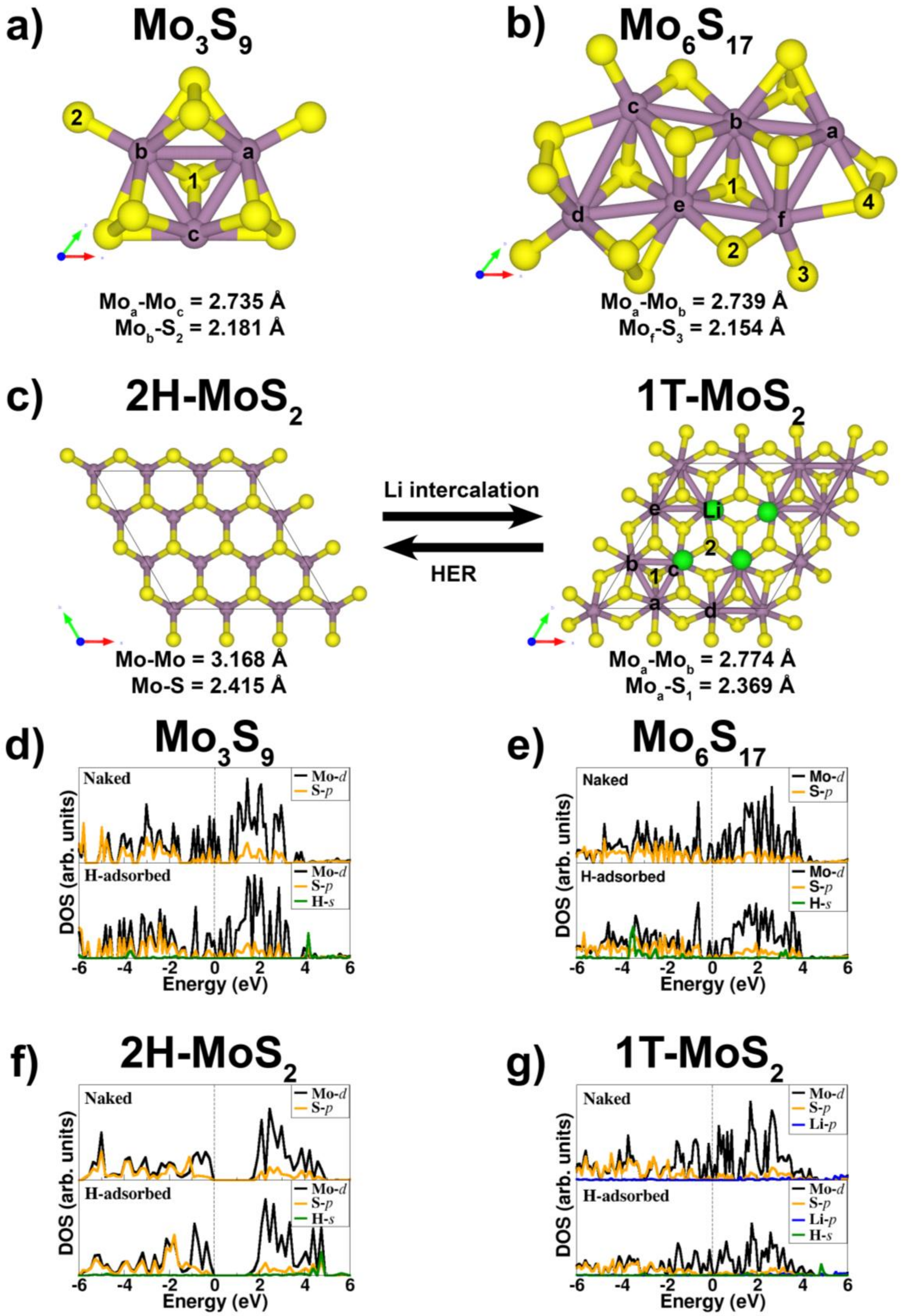

**Figure 4.** a, b) Optimized $Mo_3S_9$ (a) and $Mo_6S_{17}$ clusters serving as models for Am-$MoS_2$; c) Schematic illustration of the structural evolution between crystalline 2H and 1T $MoS_2$ phases; normalized partial density of states (PDOS) of (d) $Mo_3S_6$, (e) $Mo_6S_{17}$ clusters, (f) 2H-$MoS_2$, and (g) 1T-$MoS_2$.

In summary, we provide both experimental and theoretical evidence for the importance of a short Mo-Mo bond structure of 1T- and amorphous $MoS_2$ in comparison to crystalline 2H-$MoS_2$ for explaining the higher HER performance. While crystalline 1T-$MoS_2$ stabilized by intercalated $Li^+$ also displays high performance, Li ions will dissolve in the electrolyte during electrochemical testing, resulting in a slow transformation back to the 2H-$MoS_2$ phase and a concomitant decrease in HER activity. In contrast, amorphous $MoS_2$ retains much of its high HER activity during prolonged operation.

## Experimental Section

Experimental details can be found in the supporting information.

## Supporting Information

Supporting Information is available from the Wiley Online Library or from the author.

## Acknowledgements

This work is part of the program “$CO_2$-neutral fuels” (project 13-CO26) of the Foundation for Fundamental Research on Matter (FOM), which was financially supported by the Netherlands Organization for Scientific Research (NWO). This research program was co-financed by Shell Global Solutions International B.V. A. Sharma and A. Bol acknowledge financial support from the European Research Council (Grant Agreement No.648787-ALDof2DTMDs). Dr. Lu Gao and Jan Wiesfeld from Eindhoven University of Technology are thanked for their help in SEM measurements and 1T-$MoS_2$ preparation. Chunguang Chen and Prof. Dr. Peter H. L. Notten from Forschungszentrum Jülich, Germany are acknowledged for fruitful discussions.

## References

[1] a) D. Kong, J. J. Cha, H. Wang, H. R. Lee, Y. Cui, *Energy Environ. Sci.* **2013**, *6*, 3553-3558; b) J. Xie, J. Zhang, S. Li, F. Grote, X. Zhang, H. Zhang, R. Wang, Y. Lei, B. Pan, Y. Xie, *J. Am. Chem. Soc.* **2013**, *135*, 17881-17888; J. Xie, H. Zhang, S. Li, R. Wang, X. Sun, M. Zhou, J. Zhou, X. W. (David) Lou, Y. Xie, *Adv. Mater.* **2013**, *25*, 5807-5813.

[2] Y. Gong, Z. Liu, A. R. Lupini, G. Shi, J. Lin, S. Najmaei, Z. Lin, A. L. Elias, A. Berkdemir, G. You, H. Terrones, M. Terrones, R. Vajtai, S. T. Pantelides, S. J. Pennycook, J. Lou, W. Zhou, P. M. Ajayan, *Nano Lett.* **2014**, *14*, 442-449.

[3] Y. Yu, G. H. Nam, Q. He, X. J. Wu, K. Zhang, Z. Yang, J. Chen, Q. Ma, M. Zhao, Z. Liu, F. R. Ran, X. Wang, H. Li, X. Huang, B. Li, Q. Xiong, Q. Zhang, L. Gu, Y. Du, W. Huang, H. Zhang, *Nat. Chem.* **2018**, *10*, 638-643.

[4] K. K. Liu, W. Zhang, Y. H. Lee, Y. C. Lin, M. T. Chang, C. Y. Su, C. S. Chang, H. Li, Y. Shi, H. Zhang, C. S. Lai, L. J. Li, *Nano Lett.* **2012**, *12*, 1538-1544.

[5] X. Wang, H. Feng, Y. Wu, L. Jiao, *J. Am. Chem. Soc.* **2013**, *135*, 5304-5307.

[6] Y. Li, A. Yamaguchi, M. Yamamoto, K. Takai, R. Nakamura, *J. Phys. Chem. C* **2016**, *121*, 2154-2164.

[7] a) L. van Haandel, E. J. M. Hensen, T. Weber, *Catal. Today* **2017**, *292,* 67-73; b) L.-A. S. Carlos G. Morales-Guio, Xile Hu, *Chem. Soc. Rev.* **2014**, *43*, 6555-6569.

[8] a) J. D. Benck, T. R. Hellstern, J. Kibsgaard, P. Chakthranont, T. F. Jaramillo, *ACS Catal.* **2014**, 3957-3971; b) M. L. Tang, D. C. Grauer, B. Lassalle-Kaiser, V. K. Yachandra, L. Amirav, J. R. Long, J. Yano, A. P. Alivisatos, *Angew. Chem. Int. Ed.* **2011**, *50*, 10203-10207; c) Q. Ding, B. Song, P. Xu, S. Jin, *Chem* **2016**, *1*, 699-726.

[9] a) T. F. Jaramillo, Jørgensen, K. P., Bonde, J., Nielsen, J. H., Horch, S., Chorkendorff, I., *Science* **2007**, *317*, 100-102; b) J. C. B. H.Tributsch, *J. Electroanal. Chem.* **1977**, *81*, 97-111.

[10] a) J. Kibsgaard, Z. Chen, B. N. Reinecke, T. F. Jaramillo, *Nat. Mater.* **2012**, *11*, 963-969; b) D. Kong, H. Wang, J. J. Cha, M. Pasta, K. J. Koski, J. Yao, Y. Cui, *Nano Lett.* **2013**, *13*, 1341-1347; c) C. Tsai, H. Li, S. Park, J. Park, H. S. Han, J. K. Norskov, X. Zheng, F. Abild-Pedersen, *Nat. Commun.* **2017**, *8*, 15113.

[11] Th. Weber, J. C. Muijsers, J. W. Niemantsverdriet, *J. Phys. Chem.* **1995**, *99*, 9194-9200.

[12] C. Backes, N. C. Berner, X. Chen, P. Lafargue, P. LaPlace, M. Freeley, G. S. Duesberg, J. N. Coleman, A. R. McDonald, *Angew Chem. Int. Ed.* **2015**, *54*, 2638-2642.

[13] a) D. Voiry, A. Goswami, R. Kappera, C. de C. C. e Silva, D. Kaplan, T. Fujita, M. Chen, T. Asefa, M. Chhowalla, *Nat. Chem.* **2015**, *7*, 45-49; b) X. Geng, W. Sun, W. Wu, B. Chen, A. Al-Hilo, M. Benamara, H. Zhu, F. Watanabe, J. Cui, T. P. Chen, *Nat. Commun.* **2016**, *7*, 10672.

[14] a) Q. Tang, D.-e. Jiang, *ACS Catal.* **2016**, *6*, 4953-4961; b) Y. Yin, J. Han, Y. Zhang, X. Zhang, P. Xu, Q. Yuan, L. Samad, X. Wang, Y. Wang, Z. Zhang, P. Zhang, X. Cao, B. Song, S. Jin, *J. Am. Chem. Soc.* **2016**, *138*, 7965-7972.

[15] a) W. Chen, J. Gu, Q. Liu, R. Luo, L. Yao, B. Sun, W. Zhang, H. Su, B. Chen, P. Liu, D. Zhang, *ACS Nano* **2017**; b) M. Acerce, D. Voiry, M. Chhowalla, *Nat. Nanotechnol.* **2015**, *10*, 313-318.

[16] S. J. R. Tan, S. Sarkar, X. Zhao, X. Luo, Y. Z. Luo, S. M. Poh, I. Abdelwahab, W. Zhou, T. Venkatesan, W. Chen, S. Y. Quek, K. P. Loh, *ACS Nano* **2018**, *12*, 5051-5058.

[17] a) S. P. Cramer, K. S. Liang, A. J. Jacobson, C. H. Chang, R. R. Chianelli, *Inorg. Chem.* **1984**, *23*, 1215-1221; b) S. J. Hibble, D. A. Rice, D. M. Pickup, M. P. Beer, *Inorg. Chem.* **1995**, *34*, 5109-5113; c) M. de Boer, A. J. van Dillen, D. C. Koningsberger, J. W. Geus, *J. Phys. Chem.* **1994**, *98*, 7862-7870; d) J. Xie, Y. Xie, *ChemCatChem* **2015**, *7*, 2568-2580.

[18] a) D. Merki, S. Fierro, H. Vrubel, X. Hu, *Chem. Sci.* **2011**, *2*, 1262-1267; b) C. G. Morales-Guio, X. Hu, *Acc. Chem. Res.* **2014**, *47*, 2671-2681. c) L. Wu, N. Y. Dzade, M.

Yu, B. Mezari, A. J. F. van Hoof, H. Friedrich, N. H. de Leeuw, E. J. M. Hensen, J. P. Hofmann, *ACS Energy Lett.* **2019**, *4*, 1733-1740.

[19] a) S. J. Hibble, G. B. Wood, *J. Am. Chem. Soc.* **2004**, *126*, 959-965; b) R. I. Walton, A. J. Dent, S. J. Hibble, *Chem. Mater.* **1998**, *10*, 3737-3745; c) B. Lassalle-Kaiser, D. Merki, H. Vrubel, S. Gul, V. K. Yachandra, X. Hu, J. Yano, *J. Am. Chem. Soc.* **2015**, *137*, 314-321; d) A. Sharma, M. A. Verheijen, L. Wu, S. Karwal, V. Vandalon, H. C. M. Knoops, R. S. Sundaram, J. P. Hofmann, W. M. M. Kessels, A. A. Bol, *Nanoscale*, **2018**, *10*, 8615-8627.

[20] a) X. Li, H.-Y. Wang, H. Yang, W. Cai, S. Liu, B. Liu, *Small Methods* **2018**, *2*, 1700395; b) N. Kornienko, J. Resasco, N. Becknell, C. M. Jiang, Y. S. Liu, K. Nie, X. Sun, J. Guo, S. R. Leone, P. Yang, *J. Am. Chem. Soc.* **2015**, *137*, 7448-7455.

[21] J. W. Liwen F. Wan, Brian R. Perdue, Timothy T. Fister, Soojeong Kim, Christopher A. Apblettc, David Prendergasta, *Phys. Chem. Chem. Phys.* **2016**, *18*, 17326-17329.

[22] F. A. Lima, R. Bjornsson, T. Weyhermuller, P. Chandrasekaran, P. Glatzel, F. Neese, S. DeBeer, *Phys. Chem. Chem. Phys.* **2013**, *15*, 20911-20920.

[23] J. Liu, R. E. Saw, Y. H. Kiang, *J. Pharm. Sci.* **2010**, *99*, 3807-3814.

[24] Q. Liu, Q. Fang, W. Chu, Y. Wan, X. Li, W. Xu, M. Habib, S. Tao, Y. Zhou, D. Liu, T. Xiang, A. Khalil, X. Wu, M. Chhowalla, P. M. Ajayan, L. Song, *Chem. Mater.* **2017**, *29*, 4738-4744.

[25] K. E. Dungey, M. D. Curtis, J. E. Penner-Hahn, *Chem. Mater.* **1998**, *10*, 2152-2161.

[26] P. Afanasiev, H. Jobic, C. Lorentz, P. Leverd, N. Mastubayashi, L. Piccolo, M. Vrinat, *J. Phys. Chem. C* **2009**, *113*, 4139-4146.

[27] Z. Zeng, Z. Yin, X. Huang, H. Li, Q. He, G. Lu, F. Boey, H. Zhang, *Angew. Chem. Int. Ed.* **2011**, *50*, 11093-11097.

[28] P. D. Tran, T. V. Tran, M. Orio, S. Torelli, Q. D. Truong, K. Nayuki, Y. Sasaki, S. Y. Chiam, R. Yi, I. Honma, J. Barber, V. Artero, *Nat. Mater.* **2016**, *15*, 640-646.

[29] a) J. K. Nørskov, T. Bligaard, A. Logadottir, J. R. Kitchin, J. G. Chen, S. Pandelov, U. Stimming, *J. Electrochem. Soc.* **2005**, *152*, J23-J26; b) J. Greeley, T. F. Jaramillo, J. Bonde, I. B. Chorkendorff, J. K. Norskov, *Nat. Mater.* **2006**, *5*, 909-913.

[30] a) M. R. Gao, M. K. Chan, Y. Sun, *Nat. Commun.* **2015**, *6*, 7493; b) X. Zhao, D. Fu, Z. Ding, Y. Y. Zhang, D. Wan, S. J. R. Tan, Z. Chen, K. Leng, J. Dan, W. Fu, D. Geng, P. Song, Y. Du, T. Venkatesan, S. T. Pantelides, S. J. Pennycook, W. Zhou, K. P. Loh, *Nano Lett.* **2018**, *18*, 482-490.

[31] a) Q. Tang, D.-e. Jiang, *Chem. Mater.* **2015**, *27*, 3743-3748; b) X. Guo, G. Yang, J. Zhang, X. Xu, *AIP Adv.* **2015**, *5*, 097174; c) F. Xi, P. Bogdanoff, K. Harbauer, P. Plate, C. Höhn, J. Rappich, B. Wang, X. Han, R. van de Krol, S. Fiechter, *ACS Catal.* **2019**, *9* 2368-2380.

**Presence of shorter Mo-Mo bonds in $MoS_2$** is reported to enhance the electrocatalytic hydrogen evolution activity. Similar electronic and catalytic properties of 1T and amorphous $MoS_2$ in contrast to 2H $MoS_2$ are caused by shorter Mo-Mo and Mo-S bonds. This short Mo-Mo bond feature in 1T $MoS_2$ is caused by Li intercalation and unstable under HER conditions, whereas it is intrinsic and stable for amorphous $MoS_2$.

**Keywords**
proton reduction, $MoS_2$, polymorph, bond structure, *operando* XAS

L. Wu, A. Longo, N. Y. Dzade, A. Sharma, M. M. R. M. Hendrix, A. A. Bol, N. H. de Leeuw, E. J. M. Hensen*, J. P. Hofmann*

# The Origin of High Activity of Amorphous $MoS_2$ in the Hydrogen Evolution Reaction